Journal of Magnetism and Magnetic Materials 475 (2019) 579–585

Contents lists available at ScienceDirect

Journal of Magnetism and Magnetic Materials

journal homepage: www.elsevier.com/locate/jmmm

Research articles

Synthesis of peroxy-functionalized magnetic mesoporous silica for epoxidation of vinyl acetate

Wishulada Injumpa[a], Tanatorn Khotavivattana[b], Numpon Insin[a,c,*]

[a] Department of Chemistry, Faculty of Science, Chulalongkorn University, Bangkok 10330, Thailand
[b] Center of Excellence in Natural Products Chemistry, Department of Chemistry, Faculty of Science, Chulalongkorn University, Bangkok 10330, Thailand
[c] Center of Excellence in Materials and Bio-interfaces, Chulalongkorn University, Phayathai Road, Pathumwan, Bangkok 10330 Thailand

ARTICLE INFO

Keywords:
Heterogeneous oxidizing agent
Magnetic separation
Nanocomposite
Peroxidation
Epoxidation

ABSTRACT

Peroxy-functionalized magnetic mesoporous silica (MMS-PA) composites containing magnetic nanoparticles (MNPs) and peroxy acids were synthesized to be used as an easily reusable heterogeneous oxidant for the epoxidation of alkenes. The presence of peroxy acid functional groups on the composites was confirmed by Fourier transform infrared spectroscopy (FTIR). Transmission electron microscope (TEM) of the MMS-PA composites revealed the irregular structure of porous silica attached with the MNPs. The surface area of the MMS-PA was calculated to be 1089 $m^2 g^{-1}$, which is significantly lower than that of the starting mesoporous silica. As measured using vibrating sample magnetometer (VSM), MMS-PA exhibited saturation magnetization of 0.12 emu/g, indicating that the heterogeneous oxidant could respond to an external magnet. The oxidizing activity of the synthesized MMS-PA composites was investigated using vinyl acetate as a model substrate; the yields of the corresponding epoxide products were measured using nuclear magnetic resonance (NMR) spectroscopy. At room temperature, the freshly prepared MMS-PA gave 52% yield of the product, and the yield decreased only slightly to 47% for the recycled MMS-PA obtained by reactivating the recovered MMS-PA with concentrated H_2O_2 in acidic medium.

1. Introduction

Magnetic nanoparticles are widely used as additives in many catalysts [1–3] to facilitate the separation from reaction mixtures and control the movement of the catalysts because of their special character: superparamagnetism [4–8]. Moreover, the ease of reuse of the magnetic composite catalysts leads to the improvement in the efficiency of the magnetic composites because the materials could be recycled for several times. For instance, sulfonic acid functionalized silica-coated crystalline Fe/Fe_3O_4 core/shell magnetic nanoparticles (MNPs) was used as a catalyst in transesterification, and the nanoparticles were separated using a magnet and were reused up to five times [9]. There are many types of magnetic materials but magnetite (Fe_3O_4) and maghemite (γ-Fe_2O_3) are typically selected because they are stable in ambient condition, inexpensive, less toxic and easily synthesized [6,10–13]. In addition, nanostructures of metal ferrites (MFe_2O_4) are attractive sorbents for sorption processes due to their high stability, high surface area and excellent magnetic response [14–17].

Epoxidation is an important reaction in an industrial process for the synthesis of the epoxide, a versatile building block and intermediate in the synthesis of many valuable compounds such as pharmaceuticals, biotechnological products, adhesives or paints [18–21]. Moreover, alkenes, which are the starting materials in this reaction, are also widely used as common feedstocks in various synthetic protocols [22–24]. Typically for the epoxidation reactions, homogeneous oxidants such as *tert*-butyl hydroperoxide (*t*-BuOOH), *m*-choloperbenzoic acid (*m*CPBA) or other peroxyacids are commonly used [24,25]. Although these reagents generally gave high yield, high selectivity and also high efficiency even without catalysts, they are however difficult to separate from products [26–28].

Recently, there were a few works that demonstrated the incorporation of the organic oxidants into particles which were used as heterogeneous oxidants to simplify the separation or the purification of both oxidants and products [23,25,29]. However, there is no report that uses magnetic particles incorporated with an oxidizing agent for epoxidation. This is probably due to the fact that the strong reaction conditions (high acid concentration, high temperature and high H_2O_2 concentration) required for the synthesis of the heterogeneous oxidants were not compatible with the incorporation of the magnetic particle [23,29]. However, since magnetic particles could facilitate the

* Corresponding author.
E-mail address: Numpon.I@chula.ac.th (N. Insin).

https://doi.org/10.1016/j.jmmm.2018.11.111
Received 24 June 2018; Received in revised form 22 November 2018; Accepted 22 November 2018
Available online 23 November 2018
0304-8853/

separation process by using an external magnet [30], which is simpler and faster than filtration as magnetic separation does not require any filters or any complicate equipment for separations. Therefore, the objective of this work is to develop novel magnetic particles which are stable under strong oxidizing conditions in order to be used as an easily reusable oxidant in the epoxidation of alkenes. Our strategies include the selection of magnesium ferrite ($MgFe_2O_4$) as magnetic particles for both metals are in their stable oxidation states, the passivation the ferrite with a thin silica coating, and the adjustment of conditions for the peroxidation process.

2. Materials and methods

All chemicals were used as received without further purification. Iron(III) chloride ($FeCl_3$) (99.99%), magnesium chloride anhydrous ($MgCl_2$) (99.99%), oleic acid (90%), 1-octadecene (90%), sodium hydroxide (pellet for analysis), tetraethyl orthosilicate (TEOS; purum > 98%), 2-cyanotriethoxysilane (CTES), ammonium hydroxide (NH_4OH; 25%), methanesulfonic acid (reagent grade) were purchased from Sigma-Aldrich.

2.1. Synthesis of magnetic nanoparticles (MNPs)

Thermal decomposition technique was used for the synthesis of Mg-doped ferrite with a process previously reported with some modifications [31]. $Fe(oleate)_3$ and $Mg(oleate)_2$ mixture was first prepared as a precursor from iron(III) chloride, magnesium chloride and oleic acid. For the preparation of $Fe(oleate)_3$ and $Mg(oleate)_2$, iron(III) chloride (0.65 g, 4.0 mmol) and magnesium chloride (0.19 g, 2.0 mmol) were dissolved de-ionized (DI) water (10.0 mL), and sodium hydroxide (0.64 g, 16.0 mmol) was dissolved in DI water (10.0 mL). Then oleic acid (4.52 g, 16.0 mmol) and the sodium hydroxide solution were added into a round bottom flask, yielding the sodium oleate solution. Finally, the mixture of iron(III) chloride and magnesium chloride and a mixture of DI water:ethanol:hexane in the ratio of 12:16:28 by volume (mL) were added into the oleate solution. The mixture was refluxed at 70 °C for 4 h. Then, the mixture was extracted by of DI water (3 × 6.0 mL). $Fe(oleate)_3$ and $Mg(oleate)_2$ mixture was then dispersed in the hexane layer. The $Fe(oleate)_3$ dispersion was collected and was evaporated to obtain the $Fe(oleate)_3$ and $Mg(oleate)_2$ mixture as dark brown fluid. For the synthesis of MNPs by thermal decomposition process, a mixture of oleic acid:$Fe(oleate)_3$ and $Mg(oleate)_2$ mixture:1-octadecence of 1.0:6.0:38 by mole was prepared. The mixture was gradually heated as controlled by a temperature controller to 320 °C with the heating rate of 3.3 °C/min, and the reaction mixture was held at this temperature for 30 min under inert gas (N_2 gas). MNPs dispersion was washed several times by 2-propanol then collected using a centrifuge.

2.2. Synthesis of mesoporous silica

Sol-gel method was used to synthesize cyano-functionalized silica (MS-CN) [25,29]. First, the template was prepared using dodecylamine (30.0 g, 162 mmol) in solution of DI water (318 mL) and ethanol (312 mL). The mixture was stirred using a mechanical stirrer for 24 h. Then the mixture of TEOS (61.2 g, 294 mmol) and CTES (32.0 g, 147 mmol) (2:1 in ratio) was added dropwise to the templating mixture. The mixture was mechanically stirred for 24 h, and a thick white suspension was obtained. The suspension was then filtered, and the white solid was retained. The white solid was refluxed for three times using ethanol (600 mL) to remove the templating agent (dodecylamine). Finally, the white solid was dried at 95 °C under vacuum overnight to obtain MS-CN (white power).

For the synthesis of carboxyl-functionalized mesoporous silica (MS-COOH), the fine white solid MS-CN (30.0 g) was stirred with 65% H_2SO_4 (300 mL) at 150 °C for 3 h. After hydrolysis, the suspension was cooled down to room temperature and diluted. The solid was washed with DI water until the diluent was neutral. Then, the white powder of MS-COOH was obtained after dried at 95 °C under vacuum for 12 h.

2.3. Synthesis of magnetic mesoporous silica (MMS-COOH)

MS-COOH (12.0 g) and MNPs (6.0 mL, 31.8 g/mL) were mixed in hexane [32]. Then, the mixture was stirred overnight, and the mixture was washed with cyclohexane using centrifugation. Finally, the black solid of the MNPs and MS-COOH composite was dried at 60 °C in an oven for 3 h. To ensure the stability of the attachment, the composite was coated with a thin silica shell using a sol-gel method. 2.5 g of the composite was dispersed in ethanol (200 mL) before TEOS (1 mL) was added dropwise for 1.5 h. The mixture was stirred for 24 h, and MMS-COOH was obtained.

2.4. Synthesis of peroxy-functionalized magnetic mesoporous silica (MMS-PA or MMS-COOOH)

The peroxidation process was adapted from previous works [23,29]. Briefly, MMS-COOH (0.20 g) was mixed with methanesulfonic acid (2 mL) for 30 min at room temperature. Then, freshly prepared concentrated hydrogen peroxide (1 mL) (see Supporting Information for the preparation of the reagent) was added dropwise into the above mixture at 5 °C, and then the mixture was stirred for 12 h. Finally, the mixture was washed using a centrifuge with cold DI-water until the diluent was neutral. The solid was dried overnight under vacuum at room temperature. The MMS-PA was obtained and stored at 4 °C before use. Due to the high reactivity of this composite, the characterizations using TEM and N_2 adsorption-desorption analysis of MMS-PA were performed only after they were used in the oxidation of alkene. We called the composite as used MMS-PA for the composite after used for the first time and recycled MMS-PA for the used MMS-PA that has been reactivated with peroxidation and has been used for the second time.

2.5. Epoxidation of vinyl acetate (VA)

The typical procedure for the reaction optimization is as follows: 0.10 g of MMS-PA (2.41 mmol peroxy acid/g, 0.24 mmol) and 1.0 mL of $CDCl_3$ were first mixed for 1 min. Then, VA (1.72 mg, 0.02 mmol) was added and allowed to react for 1 h. Toluene (1.84 mg, 0.02 mmol) was added in the reaction mixture as an internal standard, and the reaction was attached with a magnet to separate solid from the solution for 2 min before reaction was completed. The solution part was collected using a syringe and filtered through a syringe filter before determining the epoxide yield using ^1H NMR technique.

2.6. Materials analyses

X-ray diffraction (XRD) patterns of samples were obtained on a DMAX 2200/Ultima + diffractometer (Rigaku, Tokyo, Japan) using Cu Kα radiation source and operating at 40 kV and 30 mA. The XRD patterns were collected with a scan range of 20°–70° for MNPs, 0°–10° for mesoporous silica with a scan speed of 1°/min. Transmission electron microscopy (TEM) images of particles were obtained using a JEM-2010 microscope at an accelerating voltage of 120 kV (Japan). The dispersed sample of MMS-COOH and MMS-PA were deposited on a carbon film with 300 mesh copper grids, and then dried in desiccators at room temperature. Fourier transform infrared (FTIR) spectra were acquired using a Nicolet 6700 (Thermo Scientific, MA, USA). A vibrating sample magnetometer (VSM, Lakeshore 7204) was used to measure the magnetic properties of the materials. The Brunauer-Emmett-Teller (BET) specific surface area and Barrett-Joyner-Halender (BJH) pore size and volume of the materials were analyzed by nitrogen (N_2) adsorption/desorption using a BEL Japan, BELSORP-mini instrument. The adsorption isotherms were determined at 77 K using highly pure N_2 as an

Fig. 1. Schematic synthesis of peroxy-functionalized magnetic mesoporous silica (MMS-PA).

adsorbate. Each sample (~0.04 g) was weighted and pretreated at 150 °C for 2 h before each measurement. The crude mixtures obtained from the epoxidation were characterized by NMR experiments performed on a Bruker Advance (III) 400WB spectrometer, and ^{1}H NMR data was used to calculate percent yield of the epoxide product.

3. Results and discussion

3.1. MMS-PA synthesis and characterization

Preparation and functionalization of the materials were achieved by a four-step process (Fig. 1): 1) thermal decomposition of iron-oleate and magnesium-oleate complexes (synthesis of MNPs), 2) cyano-functionalization of mesoporous silica (synthesis of MS-CN), 3) hydrolysis of MS-CN (preparation of MS-COOH), 4) preparation of MMS-COOH and peroxidation of MMS-COOH (synthesis of MMS-PA). Crystalline structures of the synthesized MNPs, MS-CN and MMS-COOH were characterized by XRD. The resulted XRD patterns were shown in Fig. 2 compared with the standard patterns JCPDS 19-0629, JCPDS 17-0464 and mesoporous silica patterns reported in the previous studies [23,33–35]. The XRD pattern of the MNPs matched well with a crystalline structure of magnetite (Fe_3O_4), maghemite (γ-Fe_2O_3) and magnesium ferrite ($MgFe_2O_4$), which cannot be differentiated using XRD pattern. In addition, XRD patterns of the MS-CN and MMS-COOH (Fig. 2A) showed a broad peak at 2-theta of around 2°–3°, indicating that these materials contained MCM-type of mesoporous silica as reported in the previous work [23,29]. The diffraction peaks at 2-theta around 30.0°, 35.0°, 43.0° and 62.0°, which are characteristic peaks of MNPs (magnetite maghemite and magnesium ferrite), were not observed in the XRD patterns of MMS-COOH, which might be due to the low amount of MNPs in the composites as observed in TEM images (Fig. 3c). The XRD results confirmed that MS-CN and MMS-COOH contained mesoporous silica, and the as-synthesized MNPs could contain magnetite and magnesium ferrite.

The as-synthesized MNPs were characterized further with SEM equipped with Energy Dispersive X-ray spectrometer (EDX) to estimate the amount of each element on the particles as shown in Fig. S1. According to the $MgFe_2O_4$ formula, if the MNPs are of pure $MgFe_2O_4$ phase, the Mg:Fe ratio should be 1:2, but Fig. S1 shows that the average ratio of Mg:Fe is roughly 1:10 by atom percentage, indicating that the synthesized MNPs were not pure $MgFe_2O_4$. From the observation of regular distribution of Mg signal in different areas throughout the samples without distinct phase separation (Fig. S2) and the position of XRD patterns (Fig. S3) compared with magnetite nanoparticles prepared using the same process with MNPs [31], the synthesized MNPs should be a solid solution of magnesium-doped iron ferrites. However, the as-synthesized MNPs can respond with an external magnet, meeting the requirement for our applications. The morphologies of the materials were observed using FESEM and TEM. The dispersity of MS-CN and MMS-COOH are shown in Fig. 3. FESEM images of MS-CN (Fig. 3a) and TEM image of synthesized MNPs (Fig. 3b) showed that the MNPs were of spherical shape with diameter of around 12 nm (SD = 1.28 nm, Fig. S4), while the MS-CN composites were of more irregular shape and polydispersity with the diameter of around 3.86 μm (SD = 2.18 μm, Fig. S5). The high magnification TEM images of MMS-COOH (Fig. 3d), used MMS-PA (Fig. 3e) and recycled MMS-PA (Fig. 2f) showed that the surface of large particles contained small particles of MNPs [36]. Moreover, for the TEM image of recycled MMS-PA, the small particles were aggregated, which might be caused by the loss of their surface stabilizers while exposing with the extreme oxidation conditions in the peroxidation process.

Additionally, Brunauer-Emmett-Teller (BET) nitrogen adsorption method was used to calculate surface area of MS-CN, MMS-COOH, used MMS-PA and recycled MMS-PA as shown in Table 1. Surface areas were

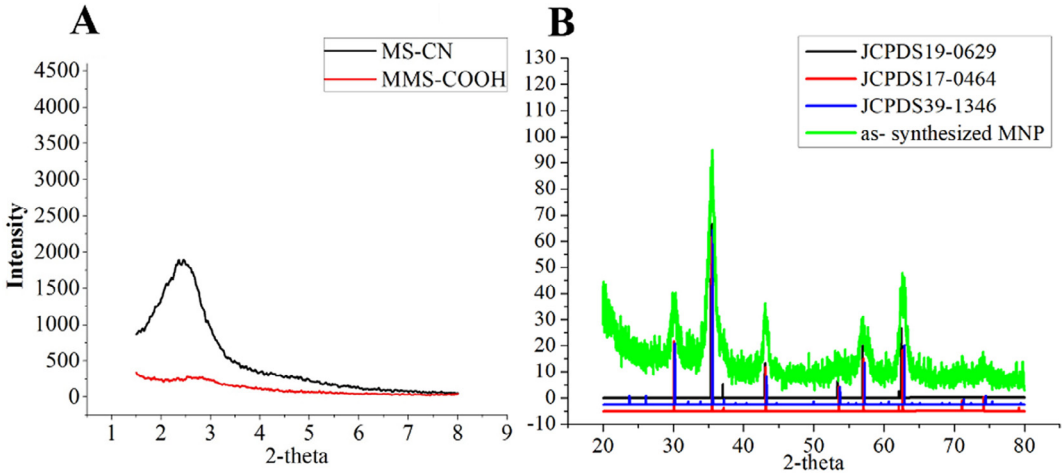

Fig. 2. The XRD patterns of MS-CN and (black A), MMS-COOH (red A) and the synthesized magnetic nanoparticles (MNPs) (green B) comparing with the standard pattern files JCPDS 19-0629 (black B) of magnetite, JCPDS 17-0464 (red B) of $MgFe_2O_4$ and JCPDS 39-1346 (blue B) of maghemite. (For interpretation of the references to colour in this figure legend, the reader is referred to the web version of this article.)

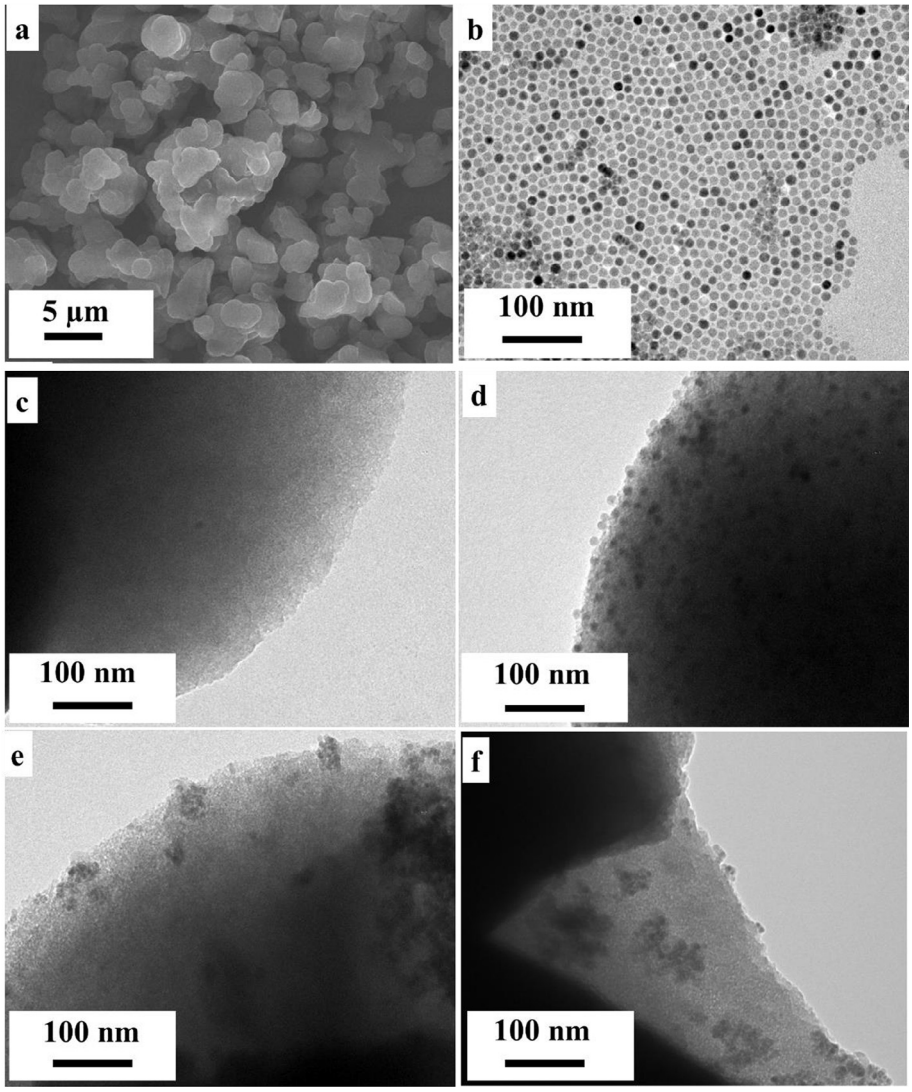

Fig. 3. (a) FESEM image of MS-CN; (b) High magnification TEM images of the synthesized MNPs, (c) MS-CN, (d) MMS-COOH, (e) used MMS-PA and (f) recycled MMS-PA.

Table 1
Textural properties of the materials.

Entry	Materials	S_{BET}[a] (m^2/g)	Pore volume[b] (cm^3/g)
1	MS-CN	1294	0.61
2	MMS-COOH	1076	0.52
3	Used MMS-PA	1089	0.35
4	Recycled MMS-PA	1025	0.24

[a] Specific surface area obtained by the BET method.
[b] Pore volume calculated from the t-plot.

$1294\ m^2/g^{-1}$, $1076\ m^2/g^{-1}$, $1089\ m^2/g^{-1}$ and $1025\ m^2/g^{-1}$ for MS-CN, MMS-COOH, used MMS-PA and recycled MMS-PA, respectively. Both mesopores and micropores were present in these composites as calculated using BJH plot and MP plot (Fig. S7 and Table S1), respectively, and the pore width distribution did not alter upon the functionalization and epoxidation processes. Surface area and the pore volume of MMS-COOH were slightly lower comparing with MS-CN, which could be caused by the interaction between the –COOH group and MNPs blocking the N_2 adsorption. Moreover, N_2 adsorption/desorption isotherm as shown in Fig. 4 displayed hysteresis loops at a relative pressure P/P_0 of 0.4–0.6, corresponding to Type IV porous materials and fitted with H_1-type hysteresis based on the IUPAC classification,

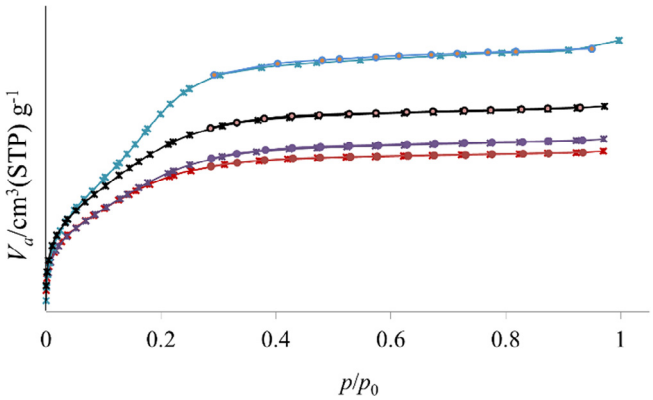

Fig. 4. N_2 adsorption/desorption isotherms of MS-CN (blue), MS-COOH (black), used MMS-PA (purple) and recycled MMS-PA (red). (For interpretation of the references to colour in this figure legend, the reader is referred to the web version of this article.)

indicating that four of the materials (MS-CN, MMS-COOH, used MMS-PA and recycled MMS-PA) possess mesoporous structure as reported previously [23,33–35].

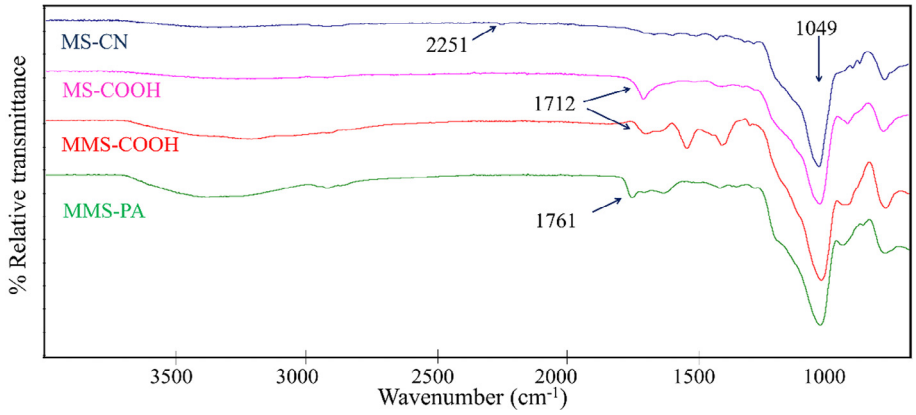

Fig. 5. IR spectra of MS-CN (blue), MS-COOH (pink), MMS-COOH (red) and MMS-PA (green). (For interpretation of the references to colour in this figure legend, the reader is referred to the web version of this article.)

Functional groups on the magnetic mesoporous silica was identified using FTIR (Fig. 5). Comparing between MS-CN and MS-COOH, only IR spectrum of MS-CN showed characteristic –C≡N stretching peak at 2251 cm^{-1}, confirming that MS-CN did contain the cyano group (–CN). After hydrolysis of MS-CN, –CN was expected to become –COOH as shown in the pink spectrum, showing the peak at 1712 cm^{-1}, which is –C═O stretching of carboxyl group, and the characteristic peak of –CN disappeared. The results indicated that the MS-CN was hydrolyzed completely and became MS-COOH. The spectrum of MMS-COOH (red) was similar with that of MS-COOH as the typical metal-oxygen (Fe-O) of Fe_3O_4 and $MgFe_2O_4$ absorption band at ~560 cm^{-1} (see Fig. S8 for the FTIR spectrum of the MNPs) was not observed because of the limitation of the IR spectrometer. The green spectrum showed the peak at 1761 cm^{-1}, which is the characteristic peak of –C═O stretching of peroxyl group, indicating that the MMS-PA consisted of peroxy acids. Moreover, the amount of peroxy on MMS-PA was calculated using iodometric titration [25,29] to be 2.41 mmol/g. According to the IR spectra and the amount of peroxy, it could be confirmed that the heterogeneous oxidant (MMS-PA) was successfully synthesized.

Magnetic property of MMS-COOH and MMS-PA before and after used (used MMS-PA) was measured using a vibrating-sample magnetometer (VSM). The magnetization under different magnetic fields of MMS-COOH and MMS-PA were as shown in Fig. 6. The saturation magnetization (Ms) of MMS-COOH is 0.34 emu/g at 25 °C, while Ms of MMS-PA and used MMS-PA are 0.12 emu/g and 0.13 emu/g at 25 °C, respectively. The low Ms values of these materials compared with Ms of the synthesized MNPs (Fig. S9) were as expected as the main components of the materials were diamagnetic silica. Amount of Fe ion of pristine MNPs and MMS-COOH were measured using ICP to evaluate MNPs loading percentage on MMS-COOH. The result shows that MNPs contain Fe equal to 122 ppm/mg and 0.79% MNPs-loading on MMS-COOH. The low MNPs-loaded percentage is in agreement with the low Ms of MMS-COOH compared with pristine MNPs. However, MMS-COOH can still be successfully removed using an external magnet.

Even though the MMS-PA underwent a harsh acidic and strong oxidizing condition of peroxidation process, it still showed magnetic response; however, the Ms of MMS-PA was decreased to roughly half of the Ms of MMS-COOH. We believe that the decrease in Ms are likely due to the dissolution and phase changes of the MNPs that were not well protected by thin silica shells, and we performed further investigation for this peroxidation process as shown in Table 2. However, the similarity in Ms of MMS-PA and used MMS-PA are likely an indicative of the similarity in MNPs component incorporated into mesoporous silica (MS) though the materials have undergone the epoxidation process. Moreover, hysteresis loops were not observed in these samples, implying a characteristic feature of a superparamagnetic behavior, which is desired in heterogeneous oxidant and heterogeneous catalyst

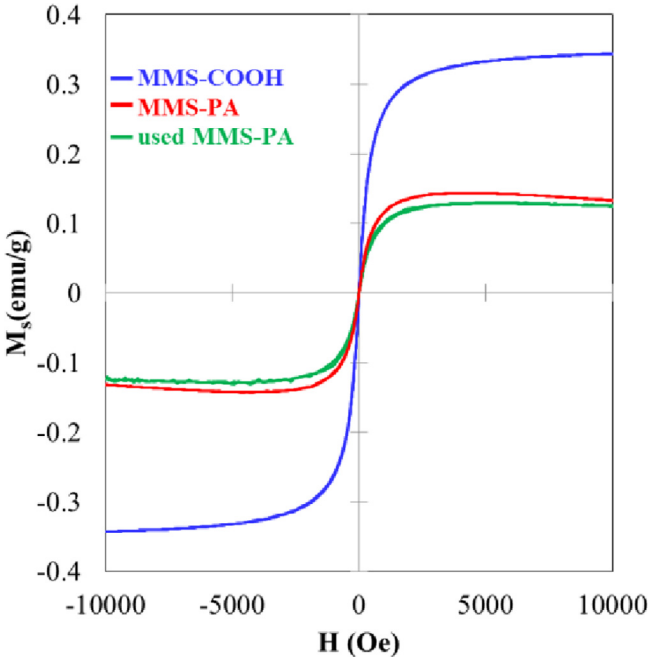

Fig. 6. Magnetization under a magnetic field of MMS-COOH (blue line) and MMS-PA before (red line) and after used (used MMS-PA) (green line). (For interpretation of the references to colour in this figure legend, the reader is referred to the web version of this article.)

applications.

Since the peroxidation process of MMS-COOH is the most important process that the balance between the oxidizing activity and the magnetic responses of MMS-PA, we optimized the condition for this process by varying the amount of H_2O_2, time and temperature as shown in Table 2. At room temperature (Entry 1), the resulted MMS-PA did not respond to a magnet potentially due to the harsh reaction conditions causing the digestion of MNPs by $MeSO_4H$. Moreover, some of the metal ions in MNPs structure might leak out from the structure and catalyzes H_2O_2 decomposition [1,37]. The issue was resolved by performing the reaction at lower temperature (5 °C) (Entry 2), yielding MMS-PA which retained the magnetism and was capable of epoxidizing VA, although the yield of the epoxide product was only 27%. Increasing the reaction time from 3 h to 6 h or 12 h did not improve the yield of the vinyl acetate epoxide product (Entries 2, 3 and 4). Finally, the MMS-PA with the most epoxidizing property (giving 48% of the epoxide product) was obtained by increasing the ratio between the H_2O_2 oxidant and the amount of the starting MMS-COOH (Entry 5); thus, the conditions

Table 2
Quantity of materials and condition used in peroxidation of MMS-COOH in relation to the yield of epoxidation.

Entry	MMS-COOH weight (g)	$MeSO_4H$ (mL)	Conc.·H_2O_2 (mL)	Time (h)	T (°C)	Magnetic-response	Epoxide-yield[a] (%)
1	0.5	2.0	0.5	3	rt.	NO	–
2	0.5	2.0	0.5	3	5	YES	27
3	0.5	2.0	0.5	6	5	YES	19
4	0.5	2.0	0.5	12	5	YES	24
5	0.2	2.0	1.0	12	5	YES	48

[a] Yield determined by ^{1}H NMR.

Table 3
Epoxidation of VA with MMS-PA.

Entry	Peroxy/VA (mol/mol)	Time (h)	T (°C)	Epoxide yield[a] (%)
1	10/1	0.5	rt.	22
2	10/1	1.0	rt.	27
3	10/1	2.0	rt.	37
4	10/1	3.0	rt.	38
5	20/1	2.0	rt.	52
6	20/1	2.0	40	64
7	20/1	2.0	50	59
8[b]	20/1	2.0	rt.	47

[a] Yield determined by ^{1}H NMR.
[b] Recycled MMS-PA.

described in Entry 5 were used for further study.

Next, the conditions for the epoxidation of vinyl acetate with the synthesized MMS-PA were optimized by varying time, temperature and the amount of MMS-PA (calculated as the overall effective mole of the peroxy acid presented) as shown in Table 3. The epoxide yield increased with longer reaction time, reaching the maximum yield of 37% at 2 h (Entries 1–4). The yield further increased to 52% when doubling the amount of the MMS-PA (Entry 5). Moreover, the yield improved to 64% when the reaction was performed at 40 °C, (Entry 6) and dropped to 59% at 50 °C (Entry 7), probably due to the decomposition of peroxy acids on the composites.

In addition, we demonstrated that the MMS-PA can be removed and recycled. A magnetic field of 3259 Oe from a rare-earth magnet was used for separating 119.8 mg of MMS-PA in 1 mL of CH_2Cl_2. After applying an external magnetic field on the epoxidation vial for 2 min, 94.6 mg of used MMS-PA was recovered from the solution as shown in Supporting information (Fig. S10) without the leftover Fe and Mg in the solution as confirmed by ICP measurement. The loss of 21% MMS-PA was likely due to the transferring and handling of the small quantity of materials. Upon the treatment of the used particles with the peroxidation conditions, the resulting MMS-PA can be used for the epoxidation of vinyl acetate, giving only slightly lower the epoxide yield of 47% at room temperature (Entry 8).

4. Conclusion

The carboxyl-functionalized mesoporous silica (MMS-COOH) which had been incorporated with magnetic nanoparticles can be oxidized in acidic media to become heterogeneous oxidant (MMS-PA) with superparamagnetic character. The MMS-PA combined the characters of high surface area (1089 m^2/g) of the MCM-type mesoporous silica and magnetization of 0.12 emu/g from the magnetic nanoparticles incorporated, even though the composites have undergone a harsh condition in presence of strong oxidizing agent. The materials can be used in the epoxidation of vinyl acetate giving the epoxide yield of 64%. The MMS-PA can be easily recovered by an external magnet and retained their efficiency when reused.

Acknowledgment

This work was financially supported by the Asia Research Center of the Korea Foundation for Advanced Studies at Chulalongkorn University (Contract Number 009/2561). Injumpa W. is supported by Science Achievement Scholarship of Thailand (SAST), Support for the Overseas Presentations of Graduate Level Academic Thesis, Overseas Research Experience Scholarship for Graduate Student and the 90th Anniversary of Chulalongkorn University Fund.

Appendix A. Supplementary data

Supplementary data to this article can be found online at https://doi.org/10.1016/j.jmmm.2018.11.111.

References

[1] S.-S. Lin, M.D. Gurol, Catalytic decomposition of hydrogen peroxide on iron oxide: kinetics, mechanism, and implications, Environ. Sci. Technol. 32 (1998) 1417–1423.
[2] M.M. Rashad, Magnetic properties of nanocrystalline magnesium ferrite by co-precipitation assisted with ultrasound irradiation, J. Mater. Sci. 42 (2007) 5248–5255.
[3] R. Sharma, S. Bansal, S. Singhal, Tailoring the photo-Fenton activity of spinel ferrites (MFe_2O_4) by incorporating different cations (M = Cu, Zn, Ni and Co) in the structure, RSC Adv. 5 (2015) 6006–6018.
[4] M. Mahmoudi, S. Sant, B. Wang, S. Laurent, T. Sen, Superparamagnetic iron oxide nanoparticles (SPIONs): development, surface modification and applications in chemotherapy, Adv. Drug Deliv. Rev. 63 (2011) 24–46.
[5] W. Injumpa, P. Ritprajak, N. Insin, Size-dependent cytotoxicity and inflammatory responses of PEGylated silica-iron oxide nanocomposite size series, J. Magn. Magn. Mater. 427 (2017) 60–66.
[6] V. Polshettiwar, R. Luque, A. Fihri, H. Zhu, M. Bouhrara, J.-M. Basset, Magnetically recoverable nanocatalysts, Chem. Rev. 111 (2011) 3036–3075.
[7] Q. Li, L. Zeng, J. Wang, D. Tang, B. Liu, G. Chen, M. Wei, Magnetic mesoporous organic–inorganic $NiCo_2O_4$ hybrid nanomaterials for electrochemical immunosensors, ACS Appl. Mater. Interfaces 3 (2011) 1366–1373.
[8] S.M. El-Sheikh, F.A. Harraz, M.M. Hessien, Magnetic behavior of cobalt ferrite nanowires prepared by template-assisted technique, Mater. Chem. Phys. 123 (2010) 254–259.
[9] H. Wang, J. Covarrubias, H. Prock, X. Wu, D. Wang, S.H. Bossmann, Acid-functionalized magnetic nanoparticle as heterogeneous catalysts for biodiesel synthesis, J. Phys. Chem. C 119 (2015) 26020–26028.
[10] G.-C. Ricardo, Y.A.-B. Asmaa, S. Iman, H.D.L. Nora, Vacancy ordering and electronic structure of γ-Fe_2O_3 (maghemite): a theoretical investigation, J. Physi. Condens. Matter 22 (2010) 255401.
[11] H.Y. Koo, S.T. Chang, W.S. Choi, J.-H. Park, D.-Y. Kim, O.D. Velev, Emulsion-based synthesis of reversibly swellable, magnetic nanoparticle-embedded polymer microcapsules, Chem. Mater. 18 (2006) 3308–3313.
[12] Y.-X.J. Wang, S.M. Hussain, G.P. Krestin, Superparamagnetic iron oxide contrast agents: physicochemical characteristics and applications in MR imaging, Eur. Radiol. 11 (2001) 2319–2331.
[13] M. Lu, M.H. Cohen, D. Rieves, R. Pazdur, FDA report: ferumoxytol for intravenous iron therapy in adult patients with chronic kidney disease, Am. J. Hematol. 85 (2010) 315–319.
[14] A.I. Ivanets, V. Srivastava, M.Y. Roshchina, M. Sillanpää, V.G. Prozorovich, V.V. Pankov, Magnesium ferrite nanoparticles as a magnetic sorbent for the removal of Mn2+, Co2+, Ni2+ and Cu2+ from aqueous solution, Ceram. Int. (2018).
[15] E.E. Ateia, A.T. Mohamed, K. Elsayed, Impact of Gd3+/graphene substitution on the physical properties of magnesium ferrite nanocomposites, J. Magn. Magn. Mater. 452 (2018) 169–178.
[16] M. Rashad, Magnetic properties of nanocrystalline magnesium ferrite by co-precipitation assisted with ultrasound, 2007.
[17] H. Hirazawa, H. Aono, K. Moritani, T. Naohara, T. Maehara, Y. Watanabe, Heat generation ability in AC magnetic field for $Y_3Fe_5O_{12}$-based garnet ferrite, IOP Conf.

Ser.: Mater. Sci. Eng. 18 (2011) 092010.
[18] X.-Y. Wang, H.-C. Shi, C. Sun, Z.-G. Zhang, Asymmetric epoxidation of cis-1-propenylphosphonic acid (CPPA) catalyzed by chiral tungsten(VI) and molybdenum (VI) complexes, Tetrahedron 60 (2004) 10993–10998.
[19] R.L. Davis, J. Stiller, T. Naicker, H. Jiang, K.A. Jørgensen, Asymmetric organocatalytic epoxidations: reactions, scope, mechanisms, and applications, Angew. Chem. Int. Ed. 53 (2014) 7406–7426.
[20] H.R. Allcock, C.J. Nelson, W.D. Coggio, Photoinitiated graft poly(organophosphazenes): functionalized immobilization substrates for the binding of amines, Proteins Metals (1994).
[21] E. Zacco, M.I. Pividori, X. Llopis, M. del Valle, S. Alegret, Renewable protein A modified graphite-epoxy composite for electrochemical immunosensing, J. Immunol. Methods 286 (2004) 35–46.
[22] W. Li, Y. Gao, W. Chen, P. Tang, W. Li, Z. Shi, D. Su, J. Wang, D. Ma, Catalytic epoxidation reaction over N-containing sp2 carbon catalysts, ACS Catal. 4 (2014) 1261–1266.
[23] M.-Y. Yao, Y.-B. Huang, X. Niu, H. Pan, Highly efficient silica-supported peroxycarboxylic acid for the epoxidation of unsaturated fatty acid methyl esters and vegetable oils, ACS Sustainable Chem. Eng. 4 (2016) 3840–3849.
[24] M. Fadhli, I. Khedher, J.M. Fraile, Modified Ti/MCM-41 catalysts for enantioselective epoxidation of styrene, J. Mol. Catal. A: Chem. 420 (2016) 282–289.
[25] R. Mello, A. Alcalde-Aragonés, A. Olmos, M.E. González-Núñez, G. Asensio, Epoxidation of olefins with a silica-supported peracid in supercritical carbon dioxide under flow conditions, J. Org. Chem. 77 (2012) 4706–4710.
[26] F. Fringuelli, R. Germani, F. Pizzo, G. Savelli, Epoxidation reaction with m-chloroperoxybenzoic acid in water, Tetrahedron Lett. 30 (1989) 1427–1428.
[27] E. Santacesaria, R. Tesser, M. Di Serio, R. Turco, V. Russo, D. Verde, A biphasic model describing soybean oil epoxidation with H_2O_2 in a fed-batch reactor, Chem. Eng. J. 173 (2011) 198–209.
[28] S. Sinadinović-Fišer, M. Janković, O. Borota, Epoxidation of castor oil with peracetic acid formed in situ in the presence of an ion exchange resin, Chem. Eng. Process.: Process Intensification 62 (2012) 106–113.
[29] J.A. Elings, R. Ait-Meddour, J.H. Clark, D.J. Macquarrie, Preparation of a silica-supported peroxycarboxylic acid and its use in the epoxidation of alkenes[dagger], Chem. Commun. (1998) 2707–2708.
[30] S.B. Hammouda, N. Adhoum, L. Monser, Synthesis of magnetic alginate beads based on Fe_3O_4 nanoparticles for the removal of 3-methylindole from aqueous solution using Fenton process, J. Hazard. Mater. 294 (2015) 128–136.
[31] J. Park, K. An, Y. Hwang, J.-G. Park, H.-J. Noh, J.-Y. Kim, J.-H. Park, N.-M. Hwang, T. Hyeon, Ultra-large-scale syntheses of monodisperse nanocrystals, Nat. Mater. 3 (2004) 891–895.
[32] B.S. Chapman, W.-C. Wu, Q. Li, N. Holten-Andersen, J.B. Tracy, Heteroaggregation approach for depositing magnetite nanoparticles onto silica-overcoated gold nanorods, Chem. Mater. 29 (2017) 10362–10368.
[33] C.-M. Yang, Y. Wang, B. Zibrowius, F. Schuth, Formation of cyanide-functionalized SBA-15 and its transformation to carboxylate-functionalized SBA-15, Phys. Chem. Chem. Phys. 6 (2004) 2461–2467.
[34] T.R. Pauly, T.J. Pinnavaia, Pore Size modification of mesoporous HMS molecular sieve silicas with wormhole framework structures, Chem. Mater. 13 (2001) 987–993.
[35] H.-Y. Lin, Y.-W. Chen, Preparation of spherical hexagonal mesoporous silica, J. Porous Mater. 12 (2005) 95–105.
[36] F. del Monte, M.P. Morales, D. Levy, A. Fernandez, M. Ocaña, A. Roig, E. Molins, K. O'Grady, C.J. Serna, Formation of γ-Fe_2O_3 isolated nanoparticles in a silica matrix, Langmuir 13 (1997) 3627–3634.
[37] T. Mimani, P. Ravindranathan, K.C. Patil, Catalytic decomposition of hydrogen peroxide on fine particle ferrites and cobaltites, Proc. Indian Acad. Sci. – Chem. Sci. 99 (1987) 209–215.